# Electric field response of ferroelectric domains near non-polar precipitates in $BaTiO_3$-based ceramics

O. Taylor,[a] E. Chaffee,[a] B.Z. Liu,[a] C. Zhao,[b,c] J. Rödel,[b] L. Zhou,[a] X. Tan[a,*]

[a]Department of Materials Science and Engineering, Iowa State University, Ames, Iowa 50011, USA

[b]Department of Materials and Earth Sciences, Technical University of Darmstadt, 64287 Darmstadt, Germany

[c]State Key Laboratory of Electrical Insulation and Power Equipment, Xi'an Jiaotong University, Xi'an 710049, P. R. China

*Author to whom correspondence should be addressed: xtan@iastate.edu

**ABSTRACT.** Precipitates have recently been found to significantly enhance the mechanical quality factor in piezoelectric ceramics. Such a piezoelectric hardening effect was attributed to strong interactions between ferroelectric domains and precipitates. In the present work, the response of domains to applied electric fields is observed *in-situ* in transmission electron microscopy in aged $(Ba,Ca)TiO_3$ ceramics with precipitates to reveal the underlying mechanism of this phenomenon. Ferroelectric domains in the Ba-rich matrix grain are observed to be more concentrated near non-polar Ca-rich precipitates. During increasing of applied voltage, domains separate from precipitates merge together first while those near precipitates persist to higher voltages. During ramping down, domains nucleate from precipitates. These direct observations confirm the strong interactions between ferroelectric domains and precipitates in piezoelectric ceramics.

**KEYWORDS:** *In-situ* TEM, Precipitates, Piezoelectric Hardening, $(Ba,Ca)TiO_3$

The piezoelectric effect is a useful property that allows for the energy conversion between mechanical and electrical forms.[1] Lead-based piezoceramics, mainly lead zirconate titanate [$Pb(Zr,Ti)O_3$, PZT] compositions, have dominated the actuator and sensor technologies.[2] However, due to the harmful effects of lead on human and environment[3], research on lead-free piezoelectrics has exploded in recent decades, with alkaline niobate-, barium titanate-, and sodium bismuth titanate-based materials being the most pursued. [4-6] In applications near resonance frequency, piezoelectric ceramics are commonly hardened with acceptor dopants to create oxygen vacancies in the lattice that impede the motion of ferroelectric domain walls.[1,7] However, the efficacy of this method is limited due to the high mobility of oxygen vacancies at moderate temperatures or large vibration velocities.[8,9] Thus, more robust methods of domain motion impedance have been explored.

Using single crystal $BaTiO_3$ as a model system, it has been demonstrated that dislocations are capable of pinning ferroelectric domain walls in place and also act as domain nucleation sites.[10] Such strong interactions not only result in significant enhancement of dielectric permittivity and large-signal piezoelectric coefficient, but also the properties are stable against electrical cycling. Volumetric defects in the form of precipitates have also been explored to manipulate electromechanical properties in $BaTiO_3$-based[7,11,12] and $(Li,Na)NbO_3$[13,14] ceramics. This piezoelectric hardening effect and other beneficial properties are also demonstrated in piezoelectric ceramic composites with intentionally mixed impurity particles.[15-19]

Piezoelectric hardening with volumetric defects is interpreted as anchoring of domain walls and restricting their motion under applied fields by the defects. However, such a micromechanism has not yet been directly observed and confirmed. In the present work, the response of ferroelectric domains to applied electric fields near non-polar Ca-rich precipitates in

a $(Ba,Ca)TiO_3$ ceramic is visualized in real time with the *in-situ* biasing transmission electron microscopy (TEM) technique. Many more domains in the Ba-rich ferroelectric matrix grain are found near precipitates; they appear to be anchored by precipitates and persist to higher applied voltages.

Ceramic pellets of $(Ba,Ca)TiO_3$ with 20 wt.% $CaTiO_3$ were prepared as described in our previous work.[7] Quenched pellets were subjected to a two-stage aging treatment for precipitate nucleation and growth. This was achieved by annealing for 72 hours at 1200ºC and then 8 hours at 1275ºC to obtain large Ca-rich precipitates that can be readily found and imaged. Annealed pellets were thinned and polished to around 150 μm thickness. Disks of 3 mm diameter were cut ultrasonically and then mechanically dimpled. After annealing at 200 ºC for 30 minutes to remove residual stresses, Argon ion milling was utilized to perforate the disk. Microstructural and chemical analysis was performed using an FEI Titan Themis 300 Cubed Scanning TEM, with its energy-dispersive X-ray spectroscopy (EDS) mapping capability used to verify composition difference between the matrix grain and the precipitates. Atomic-resolution images were taken to reveal the detailed structure at the particle/matrix interface. For *in-situ* biasing experiments, two half-circle-shaped Au films were thermally evaporated as electrodes on perforated disk specimens. Following procedures similar to our previous work,[20] *in-situ* biasing tests were performed in an FEI Tecnai G2-F20 TEM. The specialized holder, a double-tilt holder with two electric feedthroughs (Model 646.M, Gatan), was connected to a function generator for voltage adjustment. Grains of interest were aligned to the zone-axis with assistance of Kikuchi patterns, and selected area electron diffraction patterns were recorded from the matrix grain as well as precipitates. Voltage was adjusted in steps, and bright-field micrographs were taken at each voltage step to document the domain activity.

In this ceramic, Ca-rich precipitates formed during thermal annealing. They are non-polar and lose coherency after they grow into large particles. A typical precipitate, ~1.2 μm in size, is displayed in Fig. 1(a). The inset displays the electron diffraction pattern recorded from the matrix grain, indicating a $<100>_c$ zone-axis (subscript c denotes the pseudo-cubic notation). Even though the precipitate is oriented away from this direction, its interface with the matrix exhibits at least 4 straight segments, roughly along $\{001\}_c$, $\{0\bar{1}2\}_c$, $\{0\bar{3}2\}_c$ planes of the matrix grain. The high-angle annular dark-field (HAADF) STEM image of the same area is presented in Fig. 1(b). The difference in the A-site cation concentration (Ba, and Ca) is supported by EDS mapping displayed in Fig. 1(c) and (d). The precipitate particle is Ca-rich while the matrix is Ba-rich, and the composition varies sharply at the interface. High-resolution STEM imaging was performed at the area enclosed in a rectangle in (a), revealing several terraces along the interface (two are indicated by bright arrows in Fig. 1(e)) and a clear interface plane along the $\{0\bar{1}2\}_c$ plane of the Ba-rich matrix grain, Fig. 1(f). A lack of contrast in the precipitate side suggests a deviation from crystallographic axis and lower atomic number when projected along the electron beam direction.

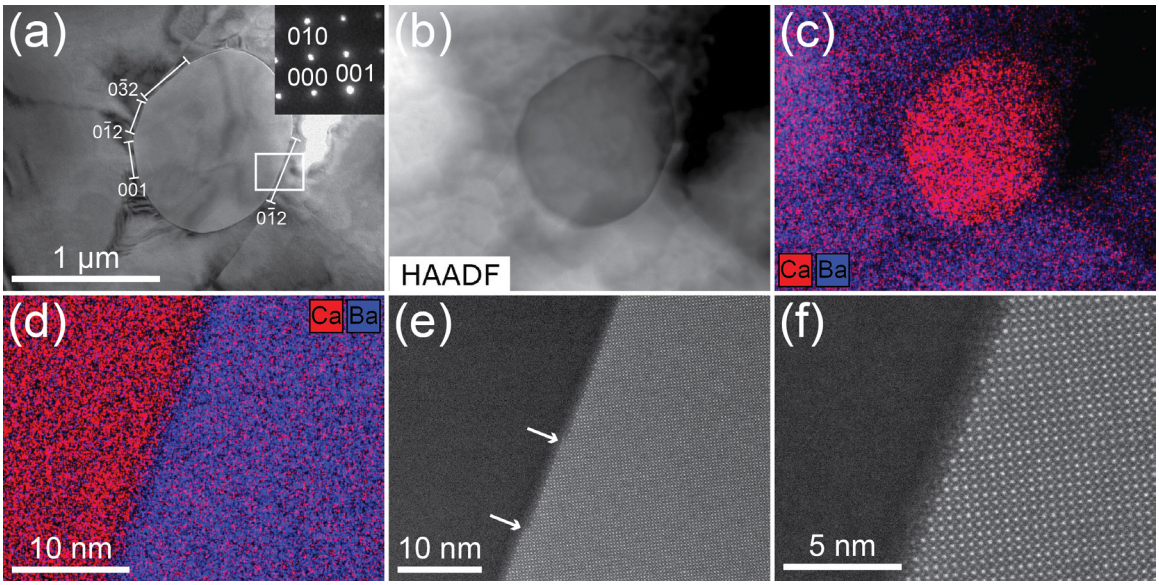


**Fig. 1** (a) Bright-field TEM image and (b) HAADF-STEM image of a Ca-rich precipitate in a <100>$_c$-oriented Ba-rich matrix grain. (c) EDS mapping of Ca and Ba elements in the same area. (d) Higher magnification EDS mapping of the rectangle area framed in (a). (e) High-resolution STEM image of the precipitate/matrix interface, with two labelled terraces. (f) Higher magnification of the same segment of interface, revealing a distinct $\{0\bar{1}2\}_c$ plane of atoms.

Another specimen was prepared, and several *in-situ* biasing experiments were performed. It should be noted that ion-mill thinning produced a major perforation with an irregular shape and many smaller holes in thin areas of this specimen. The perforation and holes drastically change the electric field distribution in the specimen.[20] As a result, the actual electric fields the grains-of-interest experience cannot be simply estimated as the voltage divided by the spacing between electrodes. Therefore, we denote the applied voltage, instead of field, at each recorded micrograph. Grain 1, containing two Ca-rich precipitate particles, was located and imaged (Fig. 2(a)). One set of coarse domains is seen both between the precipitates and terminating at precipitate I (Fig. 2(a)). Based on electron diffraction and domain wall trace analysis, the domain walls of this set are likely along the inclined $\{110\}_c$ plane. In the lower-left part of Fig. 2(a), another set of fine domains is observed with edge-on walls along the $\{01\bar{1}\}_c$ plane.

In tetragonal $BaTiO_3$ crystals, $\{101\}_c$ is energetically favored for 90° domain walls.[1,21] As only 90° and 180° domains are possible in tetragonal perovskite crystals with polar axis along the $<001>_c$ direction and the walls for 180° domains are typically wavy with very weak contrast in TEM,[21] the observed domains, with strong contrast and along $\{101\}_c$, are believed to be 90° domains in the tetragonal Ba-rich matrix grain. Due to the ambiguity in assigning polar vectors to each individual domain, we refer to these 90° domains by the crystallographic planes of their domain walls. In this specimen, 90° domains are found to be concentrated in areas next to the precipitates, indicating their formation can reduce the residual stress in the matrix grain. The differences in thermal expansion coefficients and lattice parameters between the Ca-rich precipitate and the Ba-rich matrix are the origin of residual stresses at room temperature.[1,22,23]

This specimen was first subjected to positive voltages and then negative voltages to demonstrate that the domains in Grain 1 were responsive. Bright-field micrographs were recorded in subsequent applications of voltage, with positive voltage direction marked in Fig. 2(b). Figures 2(b-f) feature the evolution of ferroelectric domains in the vicinity of the two precipitates under applied voltages. During ramping up of positive voltage, the fine $\{01\bar{1}\}_c$ domains away from the precipitates merge with the rest of the grain, partially gone at 5.8V and fully gone at 6.0V (Fig 2(b-d)). At 5.8V, the coarse $\{110\}_c$ domains remain largely unchanged, as seen in Fig. 2(b). At 5.9V in Fig. 2(c), the coarse domains which terminate at precipitate I lose contrast, but the domains with both ends anchored at the two precipitates still persist. The width of these domains is apparently reduced in Fig. 2(d) at 6.0V. All domains in Grain 1 merge into a single-domain state at 6.2V (Fig. 2(e)), which should correspond to the saturated polarization state. During ramping down of the positive voltage, $\{110\}_c$ domains with slightly different morphology reappear first between the two precipitates, as indicated by the comparison between

Fig. 2(a) and 2(f). At 0V, $\{01\bar{1}\}_c$ domains are seen again at the lower-left part of Fig. 2(f). When electric voltage of reverse polarity was applied, domains merge in a similar sequence as in the application of positive voltage. At 4.4V in reverse polarity, all domains are observed merged into a single domain with no walls visible (results not shown).

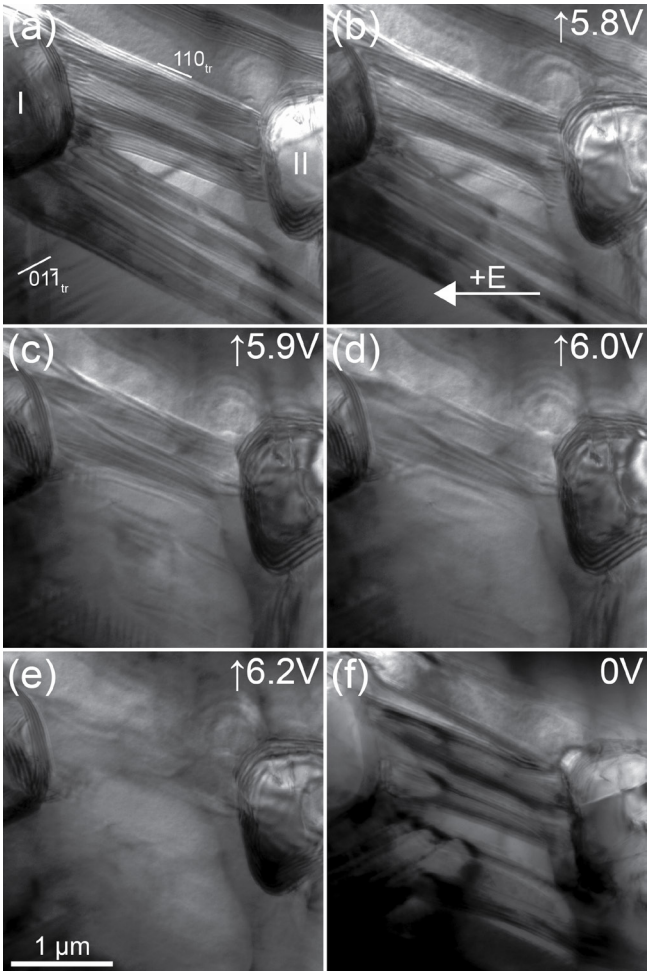


**Fig. 2** (a) Bright-field image of Grain 1 at 0V, precipitates I and II. $110_{tr}$ and $01\bar{1}_{tr}$ indicate the intersecting lines of $\{110\}_c$ and $\{01\bar{1}\}_c$ planes with the specimen surface, respectively. (b-e) Increasing applied positive voltage. (f) Zero applied voltage after positive biasing. The positive field direction is marked in (b).

The same grain was found and examined again after four days. Electron diffraction patterns of the matrix and precipitate I were recorded in this experiment and are provided in Fig.

3(a) and (b), respectively. The matrix grain is along the $<011>_c$ zone-axis while the precipitate is along its $<111>_c$ zone-axis, apparently misaligned to a large degree. The presence of superlattice diffraction spots (highlighted by the three circles in Fig. 3b) from the precipitate is consistent with results in the literature,[24] supporting that the precipitate is isostructural to $CaTiO_3$ with an orthorhombic perovskite structure.[7] Possibly due to relaxation over this period of time, a new set of fine domains formed in the lower part of Fig. 3(c), with inclined domain walls likely along $\{101\}_c$ planes. These replaced the $\{01\bar{1}\}_c$ domains in Fig. 2. Coarse $\{110\}_c$ domains are still observed between the two precipitates. *In-situ* experimentation involved ramping up and ramping down of positive voltage and results are shown in Fig. 3. Both sets of domains persist to 5.50V, as shown in Fig. 3(d). The new $\{101\}_c$ set of domains mostly merge with the rest of the grain in (e) at 5.60V. One of the domains outlined in dashed lines in Fig. 3(d-f) shows decreasing width and sideways shrinkage with increasing voltage, detaching from precipitate II while maintaining attachment to precipitate I before merging with the rest of the grain in (g). The domain below this one remains in place up to 5.68V before merging in Fig. 3(h) at 6.20V. During ramping down of the positive voltage, domains reappear first between the two precipitates at 6.10V (Fig. 3(i)), and then grow in number and width in that area at lower voltages (Fig. 3(j)).

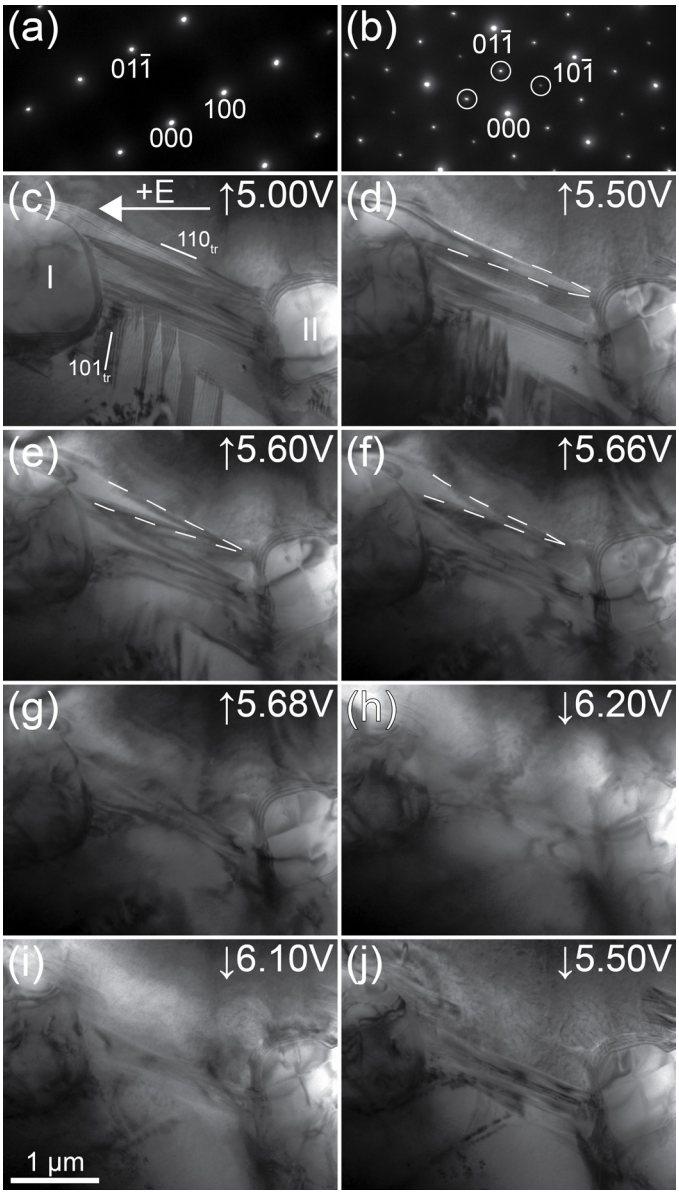


**Fig. 3** The second experimentation on Grain 1. (a) Electron diffraction pattern of Grain 1, indicating the $<011>_c$ zone-axis. (b) Electron diffraction pattern of precipitate I, indicating the $<111>_c$ zone-axis. The three circles highlight the superlattice spots. (c) Grain 1 at positive voltage, with labelled applied field direction, precipitates I and II. $110_{tr}$ and $101_{tr}$ indicate the intersection of $\{110\}_c$ and $\{101\}_c$ domain wall planes with the specimen surface, respectively. (d-g) Increasing applied positive voltage, showing domains merging. (h-j) Decreasing applied positive voltage, demonstrating reappearance of domain walls.

In the same session of the second experiment on Grain 1 (Fig. 3), another grain, Grain 2, in the same specimen was also tested (Fig. 4). As shown in Fig. 4(a), this grain has 3 visible Ca-rich precipitates, labelled I, II, and III. Electron diffraction patterns recorded from the matrix

grain and the precipitate II are displayed in Fig. 4(b) and (c), respectively. The matrix grain is on the $<011>_c$ zone-axis, and the precipitate II is on the $<010>_c$ zone axis. Ferroelectric domains are once again seen between and terminating at precipitates. While precipitates I and II appear to completely stop the domains, indicating that they likely extend through the thickness of the specimen, precipitate III appears to have domains that either go above or below it. According to the electron diffraction pattern, the domains between precipitates I and II are likely to have inclined walls along $\{101\}_c$ planes, while those between II and III have edge-on walls along $\{0\bar{1}1\}_c$ planes. Another $\{101\}_c$ domain wall can be seen in the lower part of Fig. 4(a).

The third biasing experiment also involved ramping up and ramping down of positive voltage and results are shown in Fig. 4(d) through (i). All the domains are not responsive to applied voltage up to 8.0V (Fig. 4(d)) but merge into the single-domain state at 8.5V (Fig. 4(e)). During ramping down of the positive voltage at 7.0V, domains start to form at precipitate II (Fig. 4(f)) and grow towards precipitate I at 6.8V (Fig. 4(g). At the same time, larger domains form at precipitate I (Fig. 4(g)). Further decrease in the applied voltage leads to significant growth of domains between precipitate I and II (Fig. 4(h)), and formation of domains between precipitate II and III (and stretching over III, Fig. 4(i)). In addition, apparent domain rearrangement is observed around precipitate I as well as in the lower part of Fig. 4(i). Compared to the initial domain configuration in Fig. 4(a), the $\{101\}_c$ domains between precipitate I and II are largely the same, and two new $\{0\bar{1}1\}_c$ domains appear in the lower-left area adjacent to precipitate I.

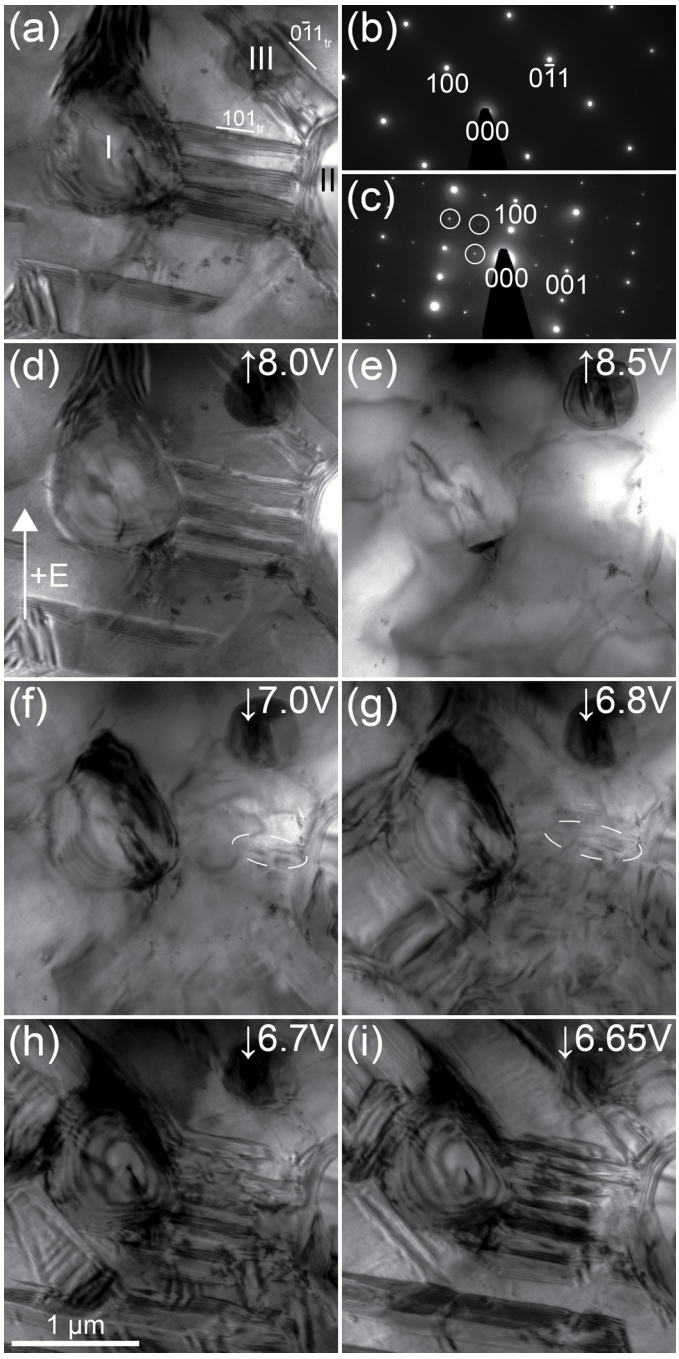


**Fig. 4** (a) Bright-field image of Grain 2, showing precipitates I-III, and $\{0\bar{1}1\}_c$ and $\{101\}_c$ sets of domains. (b) Electron diffraction pattern of Grain 2, indicating the $<011>_c$ zone-axis. (c) Electron diffraction pattern of precipitate II, indicating the $<010>_c$ zone-axis. The three circles highlight the superlattice spots. (d-e) Increasing applied voltage until complete domain merging. (f-i) Decreasing voltage leads to domain nucleation and sideways growth. The budding domain at nucleation and early growth is highlighted by the bright dashed-line ovals in (f) and (g). The positive field direction is marked in (d).

In both grains with Ca-rich precipitates, ferroelectric 90° domains in the Ba-rich matrix appear to be greatly affected by the presence of these volumetric defects. Domains are of high density between and around the precipitates, corroborating what was found in previous work on $(Ba,Ca)TiO_3$ ceramics[7] and other lead-free piezoceramics.[25] Again, their formation during cooling at the paraelectric to ferroelectric transition can effectively reduce the elastic distortion energy due to thermal residual stresses. In contrast, few domains are seen away from the precipitates in both grains. Under applied voltage, domains that are not attached to precipitates often merge with the matrix at a lower voltage compared to those attached to one or more precipitates. Furthermore, it appears that sideways domain wall motion is limited; more often domains retract along their length as they shrink to merge with the matrix domain. The merging of domains into a larger domain typically occurs within a very narrow voltage range, corresponding to the field intensity around the coercive field $E_C$ of the Ba-rich ferroelectric matrix. In addition, in grains without precipitates in the specimen, domains are often uniform in width and extend across the whole grain. During *in-situ* biasing experiments, these domains merge with one another uniformly, converting the grain into the single domain state.

During ramping down of applied voltage, domains consistently reform in the same morphology between precipitates, with several observed nucleating at one precipitate and growing into contact with another. In this case, the precipitate/matrix interface acts as nucleation points for 90° domain walls, as depicted in Fig. 4(f) and (g). This is similar to how previous work has shown dislocations to nucleate domains.[10] Domains attached only to one precipitate or completely separate from precipitates often exhibit changes in formation between *in-situ* biasing experiments. The strong association of 90° domains to precipitates not only is related to the thermal stress, but also can be attributed to the depolarization energy at the precipitate/matrix

interface due to the non-polar nature of the Ca-rich precipitate. Such an anchoring effect of the precipitate effectively restricts the domain wall motion, leading to piezoelectric hardening. In addition, the present *in-situ* biasing TEM work directly reveals the domain evolution process under applied electric fields in $BaTiO_3$, involving nucleation, lengthwise growth (retraction), sideways wall motion, and domain merging. These evolution stages are quite similar to other ferroelectric crystals.[26]

In summary, using $(Ba,Ca)TiO_3$ as a model system, ferroelectric 90° domains are directly observed interacting with precipitates under applied electric fields. The precipitates are confirmed to be Ca-rich, and hence, non-polar. The precipitate/matrix interface is often faceted even when the precipitate is large (>1 μm). The interface facets exist on $\{001\}_c$, $\{0\bar{1}2\}_c$, and $\{0\bar{3}2\}_c$ planes of the Ba-rich ferroelectric phase. A higher density of ferroelectric 90° domains is observed around Ca-rich precipitates. Application of voltage drives the domains less constrained by precipitates to merge first, with those directly attached to precipitates persist to higher voltages. Precipitates are also the favored nucleation sites for domain formation during lowering of voltage. Direct observation of this domain-precipitate interaction during biasing should help illuminate the mechanisms of precipitation hardening and inform future research into the topic.

This work was supported by the USA National Science Foundation (NSF) through Grant No. DMR-2110264.

## AUTHOR DECLARATIONS

### Conflict of Interest

The authors have no conflicts to disclose.

## Author Contributions

**Odin Taylor:** Data curation; Formal analysis; Visualization; Writing – original draft. **Ethan Chaffee:** Data curation; Methodology; Validation. **Binzhi Liu:** Data curation; Methodology. **Changhao Zhao:** Investigation; Writing – review & editing. **Jürgen Rödel:** Conceptualization; Writing – review & editing. **Lin Zhou:** Conceptualization; Data curation; Funding acquisition; Supervision; Writing – review & editing. **Xiaoli Tan:** Conceptualization; Funding acquisition; Project administration; Supervision; Writing – original draft, review & editing.

## DATA AVAILABILITY

The data that support the findings of this study are available from the corresponding authors upon reasonable request.

## REFERENCES


[1]B. Jaffe, W. R. Cook, and H. Jaffe, *Piezoelectric Ceramics*, (Academic Press, London, 1971).

[2]G. H. Haertling, J. Am. Ceram. Soc. **82**, 797-818 (1999).

[3]A. J. Bell and O. Deubzer, MRS. Bullet. **43**, 581-587 (2018).

[4]Y. Saito, H. Takao, T. Tani, T. Nonoyama, K. Takatori, T. Homma, T. Nagaya, and M. Nakamura, Nature **432**, 84-87 (2004).

[5]W. Liu, and X. Ren, Phys. Rev. Lett. **103**, 257602 (2009).

[6]T. Takenaka, K. Maruyama, and K. Sakata, Jpn. J. Appl. Phys. **30**, 2236 (1991).

[7]C. Zhao, S. Gao, T. Yang, M. Scherer, J. Schultheiß, D. Meier, X. Tan, H. Kleebe, L. Chen, J. Koruza, and J. Rödel, Adv. Mater. **33**, 2102421 (2021).

[8]M. Li, M. J. Pietrowski, R. A. De Souza, H. Zhang, I. M. Reaney, S. N. Cook, J. A. Kilner, and D. C. Sinclair, Nat. Mater. **13**, 31-35 (2014).

[9]K. Uchino, J. H. Zheng, Y. H. Chen, X. H. Du, J. Ryu, Y. Gao, S. Ural, S. Priya, and S. Hirose, J. Mater. Sci. **41**, 217-228 (2006).

[10]M. Höfling, X. Zhou, L. M. Riemer, E. Bruder, B. Liu, L. Zhou, P. B. Groszewicz, F. Zhou, B. Xu, K. Durst, X. Tan, D. Damjanovic, J. Koruza, and J. Rödel, Science **372**, 6545 (2021).

[11]F. W. Cooke, R. C. Bradt, R. C. DeVries, and G. S. Ansell, J. Am. Ceram. Soc. **49**, 648-651 (1966).

[12]M. P. Zheng, C. Zhao, and J. Rödel, Appl. Phys. Lett. **122**, 132904 (2023).

[13]C. Zhao, S. Gao, H. Kleebe, X. Tan, J. Koruza, and J. Rödel, Adv. Mater. **34**, 2202379 (2022).

[14]S. Gao, C. Zhao, M. Bohnen, R. Müller, J. Rödel, and H. Kleebe, Acta Mater. **254**, 118998 (2023).

[15]L. K.V., L. M. Riemer, J. Koruza, and J. Rödel, Appl. Phys. Lett. **111**, 022905 (2017).

[16]H. Li, H. Chen, X. Li, J. Xing, W. Liu, Z. Tan, M. Mo, N. Chen, M. Tang, and J.G. Zhu, ACS Appl. Mater. & Interf. **15**, 36576 (2023).

[17]M. Zheng, C. Zhao, X. Yan, R. Khachaturyan, F. Zhuo, Y. Hou, and J. Koruza, Adv. Func. Mater. **33**, 2301356 (2023).

[18]F. Guo, S. Dong, K. Li, J. Wang, W. Long, P. Fang, X. Li, B. Yang, and Z. Xi, J. Euro. Ceram. Soc. **14**, 4881-4887 (2022).

[19]F. Guo, Q. Zhou, Y. Chen, C. Yang, W. Bai, H. Zhou, R. Qui, W. Long, P. Fang, and Z. Xi, J. Am. Ceram. Soc. **106**, 5258-5268 (2023).

[20]X. Tan, H. He, and J. K. Shang, J. Mater. Res. **20**, 1641 (2005).

[21]Y.H. Hu, H.M. Chan, Z. Wen, and M.P. Harmer, J. Am. Ceram. Soc. **69**, 594-602 (1986).

[22]R. Ali and M. Yashima, J. Sol. St. Chem. **178**, 2867-2872 (2005).

[23]M. Yashima and R. Ali, Sol. St. Ionics **180**, 120-126 (2009).

[24]D.I. Woodward and I.M. Reaney, Acta Cryst. B**61**, 387-399 (2005).

[25]Z. M. Fan, L. Zhou, T. H. Kim, J. Zhang, S. T. Zhang, and X. Tan, Phys. Rev. Mater. **3**, 024402 (2019).

[26]V. Y. Shur, J. Mater. Sci. **41**, 199-210 (2006).